

An inverse scattering method for catheter-based optical coherence tomography

Daniel L. Marks, Tyler S. Ralston, P. Scott Carney, and Stephen A. Boppart[†]

Beckman Institute for Advanced Science and Technology and Department of Electrical and Computer Engineering, University of Illinois at Urbana-Champaign, 405 N. Mathews, Urbana IL 61801 [†]also Department of Bioengineering and College of Medicine, University of Illinois dmarks@uiuc.edu

Abstract: By physically modelling the scattering of a broadband Gaussian beam projected from an azimuthally scanned catheter, we formulate an inverse scattering solution for optical coherence tomography for intravascular or gastrointestinal imaging.

© 2005 Optical Society of America

OCIS codes: 100.3010 Image Reconstruction Techniques, 110.450 Optical Coherence Tomography

1. Introduction

The integration of optical coherence tomography (OCT) with catheters greatly increases the utility of OCT by allowing internal organs to be imaged in a minimally invasive way.[1, 2, 3, 4, 5, 6] Catheters used with OCT typically consist of a single-mode optical fiber through which the illumination beam is guided, a lens to focus the beam outside of the fiber, and a prism or cleaved surface to reflect the beam perpendicular to the long-axis of the catheter. The lens focuses the beam a fixed distance from the catheter axis. Because of this, the region of the object outside the narrow annulus where the beam is focused will be poorly resolved. In previous work [7], we showed that in the case of a laterally translated beam in OCT, an inverse scattering analysis has yielded an algorithm which allows features outside the focal region to be resolved with a resolution equivalent to that inside the focal region. We expand this work with a new analysis specific to the rotationally-scanned intravascular catheter imaging geometry.

To formulate the inverse scattering problem, we consider an object in space with a three dimensional susceptibility $\eta(\mathbf{r})$, where \mathbf{r} is expressed in the Cartesian coordinates x , y , and z . The weak scattering (Born) approximation is used, so it is assumed $\eta(\mathbf{r})$ is a weak perturbation on a background susceptibility η_0 . A broadband Gaussian beam with a numerical aperture given by NA will propagate parallel to the $x - z$ plane at an angle θ to the x axis, and will be focused a distance z_0 from the y axis. The Gaussian beam will contain illumination spatial frequencies k , where $k_L < k < k_H$, and will be rotated around the y axis for all angles $-\pi < \theta < \pi$. The beam is translated to positions $x = 0, y = p, z = 0$ along the y axis. The backscattered signal from the OCT beam is given by $S(k, \theta, p)$, from which the 3-D susceptibility $\eta(\mathbf{r})$ will be inferred. Fig. 1 illustrates this geometry. Because of the need for brevity, only the results will be summarized here. We define the following Fourier integral of the data:

$$\tilde{S}(k, n_\theta, \xi_p) = \int_{-\infty}^{\infty} \int_{-\pi}^{\pi} \exp(in_\theta\theta + ip\xi_p) S(k, \theta, p) d\theta dp \quad (1)$$

where n_θ is an integer from $-\infty < n_\theta < \infty$ and ξ_p is a spatial frequency $-\infty < \xi_p < \infty$. Furthermore, we define the following Fourier integral of the susceptibility:

$$\tilde{\eta}(k, n_\theta, \xi_p) = \int_{-\pi}^{\pi} \int_V \exp(ix\sqrt{(2k)^2 - \xi_p^2} \cos\theta + iz\sqrt{(2k)^2 - \xi_p^2} \sin\theta + i\xi_p y) \frac{\eta(\mathbf{r})}{\left(\frac{\alpha^2}{k_0^2} + i(\sqrt{x^2 + z^2 - z_0^2})\right)} d^3r \exp(in_\theta\theta) d\theta \quad (2)$$

V is taken over the volume of the object, and k_0 is the center frequency of the illumination. Defining the spectrum of the illumination is $A(k)$, and $\alpha = \pi/NA$, then the relationship between $\tilde{\eta}(k, n_\theta, \xi_p)$ and $\tilde{S}(k, n_\theta, \xi_p)$ is

$$\tilde{S}(k, \xi_p, n_\theta) = \frac{i}{2} A(k) \tilde{F}(k, \xi_p, n_\theta) \tilde{\eta}(k, \xi_p, n_\theta) \quad (3)$$

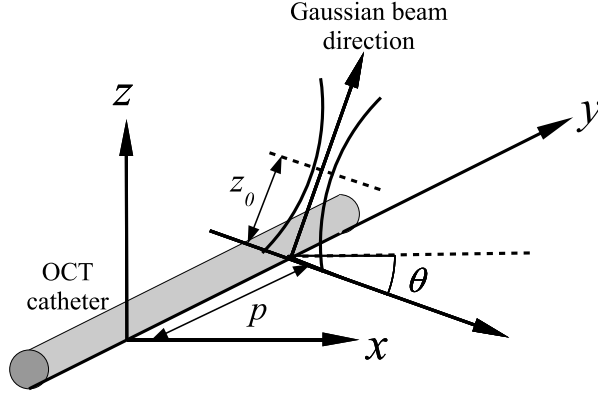


Fig. 1. Geometry of rotationally-scanned OCT catheter.

where

$$\tilde{F}(k, \xi_p, n_\theta) = \int_0^\pi d\theta \exp(i\theta n_\theta) \exp\left(-\frac{(2k)^2 \cos^2 \theta + \xi_p^2 \sin^2 \theta}{2} \frac{\alpha^2}{2k^2}\right) \exp\left(-iz_0 \sin \theta \sqrt{(2k)^2 - \xi_p^2}\right) \left(\sqrt{(2k)^2 - \xi_p^2} \sin \theta\right) \quad (4)$$

With this diagonal relationship, a Tikhonov regularized solution for the susceptibility is given by:

$$\tilde{\eta}_T(k, \xi_p, n_\theta) = \frac{-i}{2} A(k) \frac{\tilde{F}(k, \xi_p, n_\theta)^*}{|A(k) \tilde{F}(k, \xi_p, n_\theta)|^2 / 4 + F_0^2} \tilde{S}(k, \xi_p, n_\theta) \quad (5)$$

where F_0^2 is a regularization constant.

We demonstrate the inverse scattering method given by Eq. 5 by computing simulated OCT data corresponding to a collection of point scatterers, and then use the method to infer the susceptibility of the point scatterers from this synthetic data. For simplicity, we model a two-dimensional object that is uniform in the y direction. The simulated volume is 135 by 135 wavelengths and sampled every quarter wavelength, in units of the center frequency wavelength (λ_0), which is typically 800-1400 nm for OCT imaging. The fractional bandwidth of the source was 0.25. The illumination beam was $5\lambda_0$ wide at the beam waist, and was focused $38\lambda_0$ from the origin.

The synthetic data was created by choosing random positions for the point scatterers, and then summing the contributions of each scatterer at each angular direction θ and frequency k of the Gaussian beam. Rather than use the forward model of Eq. 3, the backscattered amplitude of each point was implemented in this way to validate the inverse scattering solution, which should be able to invert data produced by any correct method. This data is shown in Fig. 2 as a polar plot, and corresponds to the typical unprocessed synthetic OCT data. The dotted circle corresponds to the radius at which the Gaussian beam is focused. Point scatterers inside the annulus tend to have wavefront that curve towards the origin, and scatters outside the annulus have wavefronts that curve away from the origin.

Part (b) of Fig. 2 is the computed image from the data of part (a). The inverse was achieved using Eq. 5. The transformations in Eqs. 1 and 2 correspond to a series of coordinate changes and Fourier transforms. The coordinate changes are implemented as digital resampling of the synthetic data, and the Fourier transforms were achieved using the Fast Fourier Transform. The results show that the resolution is largely uniform and similar closer to the origin (catheter center) than the focus, but degrades progressively away from the focus. This is because the further away

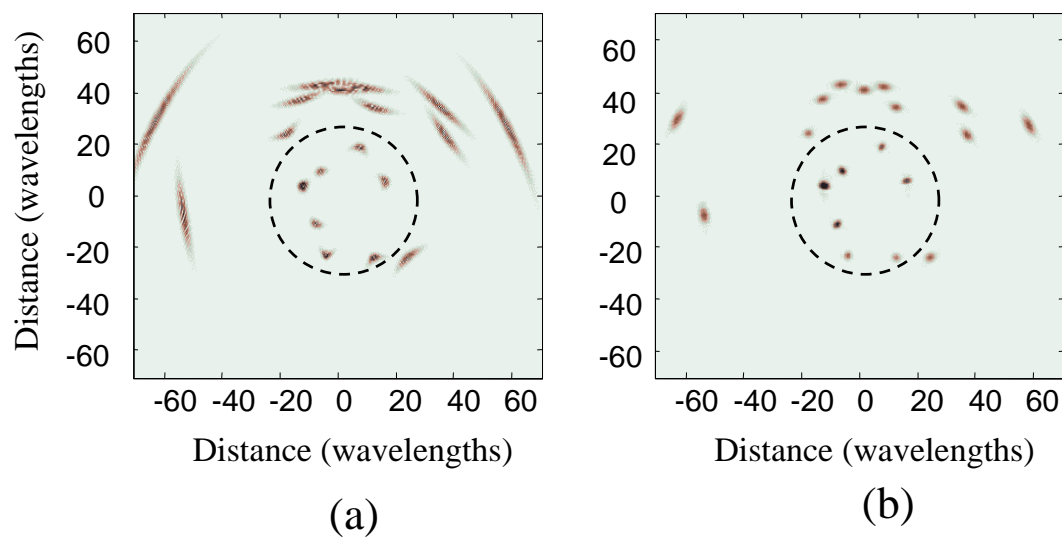


Fig. 2. Simulated (a) and reconstructed (b) OCT catheter images. Part (a) is the simulated OCT data for randomly scattered point objects. The dotted circle coincides with the focus radius of the Gaussian beam, and the center of the circle is the origin of the Gaussian beam. Part (b) is the reconstruction of the point sources from the simulated data.

from the origin, the more the outwardly curved Gaussian beam wavefronts are parallel to each other, as opposed to near the origin where the inwardly curved beams cross each other. The diversity of directions from which points near the origin are illuminated improves the achievable resolution at these points.

This method, when applied to catheter-based OCT imaging, has the potential to greatly increase the volume of the region that can be resolved without sacrificing numerical aperture. In light of this, catheters should be designed to achieve the highest transverse resolution possible, which means that the achievable resolution is limited only by the aperture size at the end of the catheter and not the depth-of-field requirement. The processing can be implemented using Fast Fourier Transform and other efficient numerical processing techniques, so a practical computational effort of $O(N \log N)$ is possible, where N is the number of resolved points.

References

1. G. J. Tearney, M. E. Brezinski, B. E. Bouma, S. A. Boppart, C. Pitris, and J. F. Southern, "In vivo endoscopic optical biopsy with optical coherence tomography," *Science* **276**(5321), 2037–2039 (1997).
2. A. M. Rollins, R. Ung-arunyawee, A. Chak, R. C. K. Wong, K. Kobayashi, M. V. Sivak Jr., and J. A. Izatt, "Real-time in vivo imaging of human gastrointestinal ultrastructure by use of endoscopic optical coherence tomography with a novel efficient interferometer design," *Opt. Lett.* **24**(19), 1358–1360 (1999).
3. F. I. Feldchtein, G. V. Gelikonov, V. M. Gelikonov, R. V. Kuranov, A. M. Sergeev, N. D. Gladkova, A. V. Shakhov, N. M. Shakhova, L. B. Snopova, A. B. Terent'eva, E. V. Zagainova, Y. P. Chumakov, and I. A. Kuznetova, "Endoscopic applications of optical coherence tomography," *Opt. Expr.* **3**(6), 257–270 (1998).
4. V. X. D. Yang, M. L. Gordon, S.-J. Tang, N. E. Marcon, G. Gardiner, B. Qi, B. Stuart, E. Seng-Yue, S. Lo, J. Pekar, B. C. Wilson, and V. I. Vitkin, "High speed, wide velocity dynamic range doppler optical coherence tomography (part III): In vivo endoscopic imaging on blood flow in the rat and human gastrointestinal tracts," *Opt. Expr.* **11**(19), 2416–2424 (2003).
5. B. E. Bouma and G. J. Tearney, "Power-efficient nonreciprocal interferometer and linear-scanning fiber-optic catheter for optical coherence tomography," *Opt. Lett.* **24**(8), 531–533 (1999).
6. I. K. Jang, B. E. Bouma, D. H. Kang, S. J. Park, S. W. Park, K. B. Seung, K. B. Choi, M. Shishkov, K. Schlendorf, E. Pomerantsev, S. L. Houser, and H. T. Aretz, "Visualization of coronary atherosclerotic plaques in patients using optical coherence tomography: comparison with intravascular ultrasound," *J. Am. Coll. Cardiol.* **39**(4), 604–609 (2002).
7. T. S. Ralston, D. L. Marks, P. S. Carney, and S. A. Boppart, "Inverse scattering problem for optical coherence tomography," *J. Opt. Soc. Am. A* **in press** (2006).